Accepted Manuscript

Poly(glycidyl methacrylate)/bacterial cellulose nanocomposites: Preparation, characterization and post-modification

Marisa Faria, Carla Vilela, Faranak Mohammadkazemi, Armando J.D. Silvestre, Carmen S.R. Freire, Nereida Cordeiro

Poly(glycidyl methacrylate)/bacterial cellulose nanocomposites: preparation, characterization and post-modification

Marisa Faria [a], Carla Vilela [b], Faranak Mohammadkazemi [c], Armando J. D. Silvestre [b], Carmen S. R. Freire [b*], Nereida Cordeiro [a*]

[a] Faculty of Exact Science and Engineering, University of Madeira, 9000-390 Funchal, Portugal

[b] CICECO – Aveiro Institute of Materials, Department of Chemistry, Campus de Santiago, University of Aveiro, 3810-193 Aveiro, Portugal

[c] Department of Cellulose and Paper Technology, Faculty of New Technologies Engineering, Shahid Beheshti University, Science and Research Campus, Zirab, Savadkooh, Mazandaran, Iran

* Corresponding authors: C.S.R. Freire (cfreire@ua.pt), N. Cordeiro (ncordeiro@uma.pt);

1

Abstract

Nanocomposites composed of poly(glycidyl methacrylate) (PGMA) and bacterial cellulose (BC) were prepared by the *in-situ* free radical polymerization of glycidyl methacrylate (GMA) inside the BC network. The resulting nanocomposites were characterized in terms of structure, morphology, water-uptake capacity, thermal stability and viscoelastic properties. The three-dimensional structure of BC endowed the nanocomposites with good thermal stability (up to 270 °C) and viscoelastic properties (minimum storage modulus = 80 MPa at 200 °C). In addition, the water-uptake and crystallinity decreased with the increasing content of the hydrophobic and amorphous PGMA matrix. These nanocomposites were then submitted to post-modification *via* acid-catalysed hydrolysis to convert the hydrophobic PGMA into the hydrophilic poly(glyceryl methacrylate) (PGOHMA) counterpart, which increased the hydrophilicity of the nanocomposites and consequently improved their water-uptake capacity. Besides, the post-modified nanocomposites maintained a good thermal stability (up to 250 °C), viscoelastic properties (minimum storage modulus = 171 MPa at 200 °C) and porous structure. In view of these results, the PGMA/BC nanocomposites can be used as functional hydrophobic nanocomposites for post-modification reactions, whereas the PGOHMA/BC nanocomposites might have potential for biomedical applications requiring hydrophilic, swellable and biocompatible materials.

2

1. Introduction

Bacterial cellulose (BC) is a cellulosic material produced by some non-pathogenic bacterial strains that shows unique properties, namely excellent mechanical strength, inherent biodegradability, biocompatibility, high water-holding capacity and high crystallinity, which allow its application as complementary nutrition [1], artificial temporary skin for wounds and burns, dental aid, artificial blood vessels and micronerve surgery, DNA separation, composite reinforcement, electronic paper, light emitting diodes and fuel cell membranes [2–6].

In recent years, particular attention has been devoted to the development of BC-based (nano)composite materials with several polymeric matrices as a result of the unique mechanical properties of BC [7–10]. Although most of the strategies that are used to obtain BC-based (nano)composites include compounding with synthetic polymer matrices, or blending with other natural polymers, the *in-situ* polymerization of monomers within the BC network is also being explored. This latter approach is particularly interesting and acrylic or methacrylic monomers such as acrylamide [11], acrylic acid [12], glycerol monomethacrylate, 2-ethoxyethyl methacrylate [13], 2-hydroxyethyl methacrylate [14], 4-styrenesulphonic acid [15], 2-aminoethyl methacrylate [16], methacryloyloxyethyl phosphate [17], methacroylcholine chloride [18], *N*-methacryloyl glycine [19] and bis[2-(methacryloyloxy)ethyl] phosphate [20], have already been polymerized within the BC network, originating functional nanocomposites for a multitude of applications spanning from ion exchange membranes for fuel cells to stimuli-responsive membranes or hydrogels for drug delivery.

Within the plethora of functional monomers, glycidyl methacrylate (GMA) is an interesting, versatile and low-cost commercial monomer that is widely used for the fabrication of epoxy methacrylic resins for application as coatings and adhesives [21].

3

Moreover, this methacrylic monomer can be used to obtain sophisticated (co)polymers by radical polymerization methods, including atom transfer radical polymerization (ATRP), reversible addition-fragmentation chain-transfer (RAFT), nitroxide-mediated polymerization (NMP) and catalytic chain transfer polymerisation (CCTP), which translates into functional materials with diverse structures and applications [22,23]. In addition to the methacrylic double bond, this reactive monomer also presents a pendent epoxy group that is inert towards radical polymerization, allowing for further functionalization of the resulting (co)polymer through the nucleophilic ring opening reactions, as discussed in detail elsewhere [23]. In fact, PGMA is considered one of the most adaptable reactive scaffolds in polymer chemistry that can be transformed into a multitude of tailored polymers [22,23]. As an illustrative example, RAFT synthesized PGMA was used as a building block for post-polymerization modifications *via* nucleophilic ring-opening reaction of the epoxy group with different nucleophilic agents, namely thiols, aromatic alcohols, sodium azide and amines, which originated a series of polymers with distinct properties [24]. Furthermore, PGMA has also been used in the development of high performance polymeric composite materials with for instance Na-montmorillonite [25], acid-modified bentonite [26] and glass fibre [27], among others.

Our interest in joining PGMA and BC aims at fabricating a nanocomposite material that can be easily submitted to post-polymerization modification to change its inherent properties. Although the grafting of GMA onto BC nanowhiskers has already been investigated for the design of reinforced poly(lactic acid)-based nanocomposites [28], the development of nanocomposites based on PGMA and BC has never been carried out before. Therefore, the present work reports the development of nanocomposites based on PGMA and BC prepared by the *in-situ* free radical polymerization of GMA, in the

4

presence and absence of a cross-linker, within the BC three-dimensional network. These PGMA-based nanocomposites were further modified by taking advantage of the acid-catalysed ring-opening reaction of the epoxy group to obtain nanocomposites based on the hydrophilic poly(glyceryl methacrylate) (PGOHMA), *viz.* a polymer prepared from an expensive monomer (glyceryl methacrylate, GOHMA). The characterization of the PGMA- and PGOHMA-based nanocomposites was performed in terms of structure, morphology, water-uptake capacity, thermal stability and viscoelastic properties.

2. Materials and Methods

2.1. Chemicals and materials

Glycidyl methacrylate (GMA, 97%, Aldrich), *N,N'*-methylenebisacrylamide (MBA, 99%, Sigma-Aldrich) and ammonium persulphate (APS, ≥98%, Sigma) were used as received. Other chemicals and solvents were of laboratory grade. Bacterial cellulose was biosynthesised in the form of wet membranes using the *Gluconacetobacter sacchari* bacterial strain [29] according to standard culture procedures [30].

2.2. Preparation of PGMA/BC nanocomposites

The *in-situ* free radical polymerization of GMA inside the BC three-dimensional network was adapted from the procedure described elsewhere [16]. First, wet BC membranes were weighed and about 60% of their water content was drained. Then, two distinct aqueous reaction mixtures were prepared: one containing GMA in a ratio of 1:2 (w_{BC}/w_{GMA}) and 0.5% APS (w/w relative to monomer), and another containing the same amounts of monomer and radical initiator, and 20% MBA (w/w relative to monomer). The drained membranes and reaction mixtures were both purged with N_2 for 30 min.

Each reaction mixture was added to the BC membranes and left for 1 h at room temperature for complete incorporation inside the BC network. The polymerization reaction took place in an oil bath for 6 h at 60 °C. The obtained nanocomposites (Table 1) were washed with distilled water during 1 h for 8 times, dried at 40 °C and stored in a desiccator until their use. For comparison purposes, samples of non-cross-linked and cross-linked PGMA were also prepared in the absence of BC.

2.3. Post-modification of the preformed PGMA-based nanocomposites

The post-functionalization of the PGMA-based nanocomposites consisted in the conversion of the epoxy groups to diol derivatives through a hot acid treatment. Briefly, the previously prepared wet PGMA-based nanocomposites (4×4 cm^2) were drained to remove excess of water and immersed in 100 mL of 0.02 M HCl aqueous solution (pH 3.5). Then, the reaction mixture was placed at 140 °C during 4 h under moderate stirring. After this period, the membranes were washed with distilled water until neutral pH, dried at 40 °C and kept in a desiccator until further use.

2.4. Characterization methods

2.4.1. Attenuated total reflection-Fourier transform infrared spectroscopy (ATR-FTIR)

The infrared spectra of the membranes were obtained using a Perkin-Elmer FT-IR System Spectrum BX spectrophotometer equipped with a single horizontal Golden Gate ATR cell after 32 scans in the 600−4000 cm^{-1} range at a resolution of 4 cm^{-1}.

2.4.2. Solid-state carbon cross-polarization/magic angle spinning nuclear magnetic resonance (^{13}C CP/MAS NMR)

The spectra were recorded on a Bruker Avance III 400 spectrometer operating at a B0 field of 9.4 T using 9 kHz MAS with proton 90° pulse of 3 μs, time between scans

of 3 seconds, and contact time of 2000 μs. A CP/MAS 4 mm solid state probe was used with an operating temperature of about 30-35 °C. ^{13}C chemical shifts were referenced with respect to glycine (C=O at δ 176.03 ppm).

2.4.3. X-ray diffraction (XRD)

The XRD measurements were carried out with a Phillips X'pert MPD diffractometer using Cu Kα radiation (λ = 1.541 Å) with a scan rate of 0.05° s^{-1}(in 2θ scale). The peaks were deconvoluted using Pearson VII peak functions (Peakfit software) for crystallinity index, I_C,:

$$I_C = 1 - \frac{I_{am}}{I_{002}} \times 100\%$$

where I_{002} is the maximum peak intensity at 2θ around 22°, representing the crystalline region of cellulose, and I_{am} is the minimum peak intensity at 2θ around 18°, representing the amorphous region of cellulose [31].

2.4.4. Scanning electron microscopy (SEM)

Scanning electron micrographs of the surface and cross-section of the samples were obtained by scanning electron microscopy (SEM) with a HR-FESEM SU-70 Hitachi microscope operating at 4 kV in the field emission mode. Before analysis, the samples were deposited on a steel plate and coated with carbon.

2.4.5. Water-uptake capacity

The water-uptake (*W*U) of the nanocomposites was determined by immersing the samples (1×1 cm^2) in distilled water at room temperature with a minimum of three replicas. The weight increase was periodically measured for a period of 48 hours. For each measurement, the samples were taken out of the water, their wet surfaces

immediately wiped dry with filter paper, weighed, and then re-immersed. The water-uptake was calculated using the equation:

$$WU(\%) = \frac{(W_w - W_0)}{w_0} \times 100\%$$

where, W_w is the sample weight after immersion in water and W_0 is the initial weight of dry sample.

2.4.6. Thermogravimetric analyses (TGA)

Thermal stability was evaluated with a SETSYS Setaram TGA analyser equipped with a platinum cell. Samples (*ca*. 10 mg) were heated at a constant rate of 10 °C min⁻¹, from room temperature to 800 °C, under a nitrogen flow of 20 mL min⁻¹.

2.4.7. Dynamic mechanical analyses (DMA)

The viscoelastic properties were analysed on a Tritec 2000 DMA equipment (Triton Technologies) using tension as deformation mode (single strain). For the temperature sweeps, a ramp rate of 2 °C min⁻¹ was used and samples (0.5×3.0 cm²) were heated from −40 to 200 °C, at a frequency of 1 Hz with a displacement of 0.005 mm.

3. Results and Discussion

Two different nanocomposites based on PGMA and BC were prepared through the *in-situ* free radical polymerization of GMA inside the three-dimensional network of BC using APS as radical initiator. PGMA was selected because it is a stable hydrophobic polymer whose storage under room temperature and ambient conditions can last for years without any evidence of degradation [23]. One of the nanocomposites was prepared without a cross-linker (*i.e*. PGMA/BC), while for the other MBA was utilized as cross-linking agent (*i.e*. PGMA-MBA/BC) to assess the impact of using a cross-

8

linked and a non-cross-linked PGMA matrix on the properties of the nanocomposites. The cross-linker (type and amount) was selected based on previous studies [10,16]. The reaction schemes of the PGMA polymerization in the presence and absence of cross-linker are displayed in Fig. 1.

In general, both nanocomposites (PGMA/BC and PGMA-MBA/BC) display macroscopic homogeneity with no visible irregularities on either side of the membranes surface. Moreover, the nanocomposites were whiter and less translucent than pure BC (Fig. 2). No sensible differences were discernible among nanocomposites regarding the effect of the absence or presence of cross-linker. The two nanocomposites were characterized in terms of structure (FTIR and ^{13}C CP/MAS NMR), crystallinity (XRD), morphology (SEM), water-uptake capacity, thermal stability (TGA) and viscoelastic properties (DMA). After the *in-situ* polymerization and given that the epoxy function is stable during radical polymerization, the preformed nanocomposites were treated with hot hydrochloric acid to convert the epoxy rings into diol functional groups (Fig. 1c). The ensuing nanocomposites, PGOHMA/BC and PGOHMA-MBA/BC, remained whitish and with low translucency, and were also characterized by the above-mentioned techniques. Since PGOHMA is a water-soluble polymer, the presence of a cross-linked or non-cross-linked polymer inside the BC three-dimensional network will impact the polymer migration out of the material when in contact with water, as already verified for other BC-based nanocomposites [18].

3.1. Structural and morphological characterization

The analysis of the FTIR-ATR spectra (Fig. 3) of the nanocomposites was an easy way to bear out the occurrence of the GMA polymerization inside the BC network, as well as to confirm the stability of the epoxy moiety during the radical polymerization.

9

The FTIR spectrum of the cross-linked PGMA (Fig. 3a) was consistent with the expected structure, showing all the relevant bands at 3350 cm^{-1} (OH stretching of physisorbed moisture and N–H stretching from the cross-linker), 2994 and 2946 cm^{-1} (C–H stretching), 1724 cm^{-1} (C=O stretching), 1252, 906 and 844 cm^{-1} (C–O–C epoxide ring stretching) [32–34]. The FTIR spectrum of BC (Fig. 3b) displays the characteristic absorption bands of the cellulose backbone, *viz.* 3340 cm^{-1} (O–H stretching), 2900 cm^{-1} (C–H stretching), 1310 cm^{-1} (O–H bending) and 1030 cm^{-1} (C–O stretching) [2]. The FTIT-ATR spectra of the PGMA-based nanocomposites clearly resemble the sum of the vibration peaks of the individual components, and the presence of the bands assigned to the oxirane ring supports the stability of the epoxy moiety during the free radical polymerization. Moreover, the absence of the band at about 1630 cm^{-1} allocated to the C=C stretching of the methacrylic group [33,35] of the monomer (and of the cross-linker in the case of PGMA-MBA/BC), confirms the occurrence of the *in-situ* free radical polymerization of GMA.

The solid-state ^{13}C CP/MAS NMR spectroscopy also confirmed the composition of the nanocomposites through the presence of the typical resonances of both PGMA and BC. According to Fig. 4, PGMA/BC and PGMA-MBA/BC nanocomposites exhibit the resonances of the cellulosic substrate at δ 65.2 ppm (C6), 71.7–74.5 ppm (C2, C3, C5), 89.0 ppm (C4) and 105.1 ppm (C1) [36], jointly with those of the PGMA at δ 16.8 ppm (CH$_3$ of polymer backbone, C3'), 44.9 ppm (quaternary C of polymer backbone, C2', and CH$_2$ of polymer backbone, C1'), 49.2 ppm (CH$_2$ of the epoxide ring, C7'), 54.8 ppm (CH of the epoxide ring, C6'), 67.1 ppm ((O=)COCH$_2$, C5') and 177.4 ppm (C=O, C4') [37]. The absence of the methylene carbon resonance (–NHCH$_2$NH–) of the cross-linker may be due to the lower content used in the polymerization reaction. In addition, the non-appearance of the carbon resonances associated with the double bond (C=C) of

10

the methacrylic group of GMA [38] and of the cross-linker (MBA) in the case of PGMA-MBA/BC, is another evidence of the occurrence of the *in-situ* polymerization of GMA, as formerly indicated by FTIR-ATR.

Fig. 5 displays the XRD profiles of pure BC, and PGMA/BC and PGMA-MBA/BC nanocomposites. The diffraction pattern of BC (Fig. 5a) shows the three characteristic reflections of cellulose I (native cellulose) at *ca. 2θ* 14.8º, 16.9º and 22.9° corresponding to the (100), (010) and (110) crystallographic planes [39], whereas PGMA and cross-linked PGMA exhibited a diffraction profile characteristic of amorphous polymeric materials, in good agreement with previously published data [40]. On the other hand, the nanocomposites diffractograms kept the main features of cellulose but the intensity of the peaks at *ca. 2θ* 14.8º and 16.9º decreased relatively to the (110) crystallographic plane, which might be an indication of higher disorder in the inter-sheet spacing with the addition of PGMA [41]. A similar behaviour was observed for nanocomposites of a poly(ionic liquid) and BC [18]. Furthermore, the crystallinity index (I_c) of the nanocomposites increased with the increasing content of BC ($I_c = 65$–79% [2]) from 56% for the nanocomposite containing 33% of BC (PGMA-MBA/BC) to 69% for the nanocomposite containing 39% of BC (PGMA/BC). This data agrees with the XRD patterns depicted in Fig. 5.

Fig. 6 shows the SEM micrographs of the surface and cross-section of pure BC and PGMA-based nanocomposites. The three-dimensional nanofibrillar network and lamellar microstructure representative of the BC morphology are not clearly perceptible on the surface and cross-section of the nanocomposites. In fact, the BC nanofibrils are completely embedded and the lamellar spaces are occupied with PGMA, which is particularly visible in the case of PGMA-MBA/BC. The cross-section micrographs show the effect of the absence and presence of cross-linker with PGMA-MBA/BC

11

depicting the formation of irregular-shape and micron-size particles of cross-linked PGMA. Although both nanocomposites have a similar matrix content (61 wt.% PGMA for PGMA/BC and 67 wt.% PGMA for PGMA-MBA/BC), the use of a cross-linker favored the formation of more porous material.

3.2. Water-uptake capacity

The rehydration ability of the PGMA-based nanocomposites was evaluated by immersing these materials in water during 48 h at room temperature. The PGMA/BC and PGMA-MBA/BC nanocomposites show similar water-uptake values of $32.8 \pm 2.7\%$ and $31.4 \pm 8.7\%$, respectively, which is in line with the PGMA hydrophobicity [10]. Despite the hydrophilic nature of BC with a water-uptake capacity of $138 \pm 6.4\%$, the low amount of this cellulosic substrate on the nanocomposites, *i.e*. 39% for PGMA/BC and 33% for PGMA-MBA/BC, originated materials with low water-uptake values. A similar trend was observed for example for PGMA/Na–montmorillonite nanocomposites, whose water-uptake capacity was about 35% for a nanocomposite containing 62 wt.% of GMA and 38 wt.% of the hydrophilic clay [25]. The water-uptake capacity of these nanocomposites will influence their performance depending on the type of final application.

3.3. Thermal stability

The thermal stability and degradation profile of the PGMA-based nanocomposites and the corresponding individual components were studied by thermogravimetric analysis in nitrogen atmosphere, as depicted in Fig. 7. The native BC, in addition to the dehydration below 100 °C (loss of *ca*. 4 wt.%), exhibits a single step degradation profile with initial and maximum decomposition temperatures at 266 and 347 °C (Fig. 7a),

respectively, in good agreement with previously published data [17]. PGMA (not shown) and cross-linked PGMA (Fig. 7a) present a comparable degradation profile with two consecutive weight-loss steps. In addition, both exhibit an initial loss allocated to the release of adsorbed water (loss of *ca*. 1.4 wt.%), in line with data reported elsewhere [40,42]. The cross-linked PGMA started to decompose close to 278 °C and reached the two maximum decomposition temperatures at about 352 °C and 402 °C, which correspond to the depolymerization to monomer and ester decomposition [43].

The TGA profile of PGMA-based nanocomposites followed a three-step weight-loss with initial decomposition temperatures at *ca*. 270 °C for both nanocomposites. It is clear from the data displayed in Fig. 7b that the first step at 324 °C for PGMA/BC and 336 °C for PGMA-MBA/BC is associated with the degradation of the cellulose skeleton, and the second (364 °C for PGMA/BC and 368 °C for PGMA-MBA/BC) and the third steps (414 °C for PGMA/BC and 408 °C for PGMA-MBA/BC) can be attributed to the degradation of PGMA polymer backbone, corresponding to about 17 and 32 wt.% of the initial mass for PGMA/BC and PGMA-MBA/BC, respectively. A weight-loss of about 88 and 96 wt.% was obtained for PGMA-MBA/BC and PGMA/BC, respectively, at temperatures up to 800 °C. Worth noting is the fact that the use of a cross-linking agent marginally affects the thermal stability of the ensuing nanocomposites.

3.4. Viscoelastic properties

The viscoelastic properties of PGMA/BC and PGMA-MBA/BC nanocomposites were evaluated through DMA and the corresponding data in terms of storage modulus (*E'*) and loss factor (tan *δ*) is summarized in Fig. 8. These properties were not assessed neither for PGMA nor cross-linked PGMA owing to their low film-forming capacity.

Regarding the pure BC, the variation of E' as a function of temperature (not shown) has almost no fluctuations, being relatively stable up to at least 200 °C, as discussed in detail elsewhere [15].

In the case of the nanocomposites, the temperature dependence of E' show distinct regions with different decreasing slopes. Nanocomposite PGMA/BC displays a reduction in E' from 620 MPa at −40 °C to 410 MPa at 40 °C, followed by a steep drop to 115 MPa at 120 °C, and then another decrease to 80 MPa at 200 °C. Nanocomposite PGMA-MBA/BC presents a similar pattern with E' decreasing from 675 MPa at −40 °C to 430 MPa at 60 °C, then to 230 MPa at 135 °C and finally to 140 MPa at 200 °C. As expected, the storage modulus of the nanocomposite containing the cross-linked PGMA (*i.e*. PGMA-MBA/BC) is higher than the non-cross-linked counterpart (*i.e*. PGMA/BC) for the entire temperature range, which points to a material with better viscoelastic properties. Even though E' drops from 620 MPa (−40 °C) to 80 MPa (200 °C) for PGMA/BC and from 675 MPa (−40 °C) to 140 MPa (200 °C) for PGMA-MBA/BC, the nanocomposites still maintain a reasonable mechanical integrity endowed by the micro- and nano-fibrillar structure of BC. This behaviour was indeed shown for other BC-based nanocomposites with hydrophilic polymeric matrices such as poly(4-styrene sulfonic acid) [15] and poly(methacryloyloxyethyl phosphate) [17], as well as hydrophobic matrices like for example Nafion® perfluorinated resin [44].

The loss tangent (tan δ) confirms the temperature dependence of E' with both nanocomposites presenting a broad peak in the range -40 to 200 °C, as displayed in Fig. 8. The maximum of tan δ at about 92 °C for PGMA/BC and 96 °C for PGMA-MBA/BC corresponds to the glass α-transition temperature (T_g) with an obvious correlation with the T_g value (96 °C, determined by DSC (differential scanning calorimetry)) reported

14

for PGMA homopolymer [45], which reflects the hard and brittle nature of these nanocomposite materials at room temperature.

3.5. Post-modification of the preformed PGMA-based nanocomposites

The presence of the highly reactive oxirane ring in the polymer side-chains of PGMA allows it to undergo further functionalization by the well-known nucleophilic ring-opening reaction of the epoxy group [23]. As an example, Gao et al. (2010) synthesized linear and star-shape PGMAs by atom transfer radical polymerization followed by functionalization with four different amines by ring-opening addition to obtain poly(glyceryl methacrylate) (PGOHMA) derivatives with distinct water-solubility [46]. The hydrophilic and water-soluble PGOHMA is a particularly interesting polymer for myriad applications that is prepared from a relatively expensive specialty monomer, *viz.* glyceryl methacrylate. Alternatively, PGOHMA can be prepared by the acid-catalysed hydrolysis of precursor polymers, including poly(solketal methacrylate) [47,48]. Nevertheless, the acid-catalysed hydrolysis of PGMA [23,49] is a less expensive pathway due to the commercial availability of GMA [21].

In the present study, the acid-catalysed post-modification of the preformed PGMA/BC nanostructured materials was chosen as a possible route to generate nanocomposites based on PGOHMA to widen the application range of these materials. The treatment of the preformed PGMA-based nanocomposites with hot hydrochloric acid (pH 3.5) originated white PGOHMA-based nanocomposites (Fig. 2) with higher water-uptake values, namely 178 ± 3.4% for PGOHMA/BC and 222 ± 1.2% for PGOHMA-MBA/BC, because of the hydrophilic and swellable nature of PGOHMA. These values are comparable for example with the data reported for BC-based

nanocomposites prepared by the same approach but with the hydrophilic and swellable poly(2-hydroxyethyl methacrylate) (PHEMA) as matrix [14]. In addition, the high water-uptake values of the hydrophilic PGOHMA-based nanocomposites are a major asset since it might allow *e.g.*, the absorption of exudates or other body fluids when adhered to the skin surface.

The FITR-ATR spectra of the nanocomposites after post-modification did not show any bands allocated to the epoxy ring, which was further confirmed by solid-state ^{13}C NMR spectroscopy. The ^{13}C CP/MAS NMR spectra of the of PGOHMA-based nanocomposites displayed in Fig. 9 depict the carbon resonances of BC (Fig. 4b), as well as those of PGOHMA at δ 16.3 ppm (CH$_3$ of polymer backbone, C$_c$), 45.2 ppm (CH$_2$ of polymer backbone, C$_a$, and quaternary C of polymer backbone, C$_b$), 60.9 ppm (OCH$_2$CH(OH)CH$_2$OH, C$_g$), 63.5 ppm (OCH$_2$CH(OH)CH$_2$OH, C$_e$), 70.7 ppm (OCH$_2$$C$H(OH)CH$_2OH, C_f$) and 178.8 ppm (C=O, C$_d$) [49,50]. The reduction/absence of the methine and methylene carbon resonances of the epoxide ring (Fig. 4a) demonstrates the occurrence of the ring opening reaction of the epoxide group (*i.e.* acid-catalysed hydrolysis) into the corresponding diol derivative. Worth noting is the fact that, despite the reported occurrence of isomerization during the acid-catalysed epoxy opening of PGMA that yields PGOHMA with 2,3-diol or 1,3-diol units [49], here, only the 2,3-isomer was obtained (Fig. 9).

The acidic heat treatment decreased the degree of crystallinity of the resulting nanocomposites. According to the XRD data, the diffraction peaks of BC are still observed, however, the I_c diminished from 69% (PGMA/BC) to 38% for PGOHMA/BC and from 56% (PGMA-MBA/BC) to 43% for PGOHMA-MBA/BC. This might be an indication that the BC crystalline structure was affected by the acid treatment. Despite the augment of the amorphous character of the nanocomposites after the acidic heat

16

treatment, one might infer from the previous results (ATR-FTIR and ^{13}C CP/MAS NMR) that the post-modification conditions (0.02 M HCl, 140 °C, 4 h) did not promote the hydrolysis of cellulose or at least not to a significant extent. In fact, the presence of all the carbon resonances allocated to the cellulosic substrate (see Fig. 8) and the preservation of the mechanical integrity of the membranes after the acid-catalysed hydrolysis of the preformed PGMA polymer (see Fig. 2), corroborates the hypothesis of non-occurrence of hydrolysis of BC.

The simple visual inspection of the SEM micrographs (Fig. 10) also shows the embedment of the nanofibrils and the filling of the lamellar spaces of BC with non-cross-linked and cross-linked PGOHMA, which is a possible indication of the good compatibility between the hydrophilic PGOHMA and BC.

The thermal degradation profile of the nanocomposites after heat treatment changed to a two-step degradation pathway, as illustrated in Fig. 11. Besides the water evaporation below 100 °C (loss of about 3 wt.%), both nanocomposites are thermally stable up to 250 °C (loss of 6–7 wt.%), which is a good indication that these nanomaterials have a thermal stability that comply with for example the sterilization conditions. The first stage with maximum decomposition temperature of 338 °C for PGOHMA/BC and 333 °C for PGOHMA-MBA/BC is comparable to the degradation of the cellulose skeleton, whereas the second stage between 385 and 450 °C for both nanocomposites corresponds to the degradation of the PGOHMA polymer backbone [47]. These results show that the acidic treatment had no significant effect on the thermal stability of the nanocomposites, regardless of the presence or absence of a cross-linking agent. Although both nanocomposites were dried prior to analysis, the hydrophilic nature of PGOHMA is visible on the thermal degradation profile of these

17

materials (Fig. 11) as evidenced by the dehydration step at *ca*. 100 °C with a loss 2 times higher than the value obtained for the hydrophobic PGMA (Fig. 7).

Fig. 12 shows the variation of E' and tan δ with temperature for the PGOHMA-based nanocomposites. After the post-modification, the ensuing nanocomposites behave differently with the E' of PGOHMA/BC decreasing monotonically from 1.13 GPa at -40 °C to 230 MPa at 200 °C, and the E' of PGOHMA-MBA/BC showing three regions with different decreasing slopes: from 429 MPa at −40 °C to 252 MPa at 50 °C, followed by a small plateau until 80 °C, after which E' drops to 171 MPa at 200 °C. The comparison of this data with the results obtained for the PGMA-based nanocomposites points out a distinct trend for E' (Fig. 8). PGOHMA/BC presents higher E' values than PGMA/BC for the entire temperature range, while in the case of PGOHMA-MBA/BC the E' values are lower than PGMA-MBA/BC in the temperature range of -40 to 140 °C, but then higher until reaching 200 °C. This translates into brittle materials at room temperature with E' values of 767 MPa for PGOHMA/BC and 283 MPa for PGOHMA-MBA/BC (Fig. 12). Nevertheless, these hydrophilic and swellable nanomaterials are satisfactorily pliable and workable for application *e.g.* as hydrogels for the delivery of drugs or bioactive compounds.

Regarding the tan δ, PGOHMA/BC is dominated by a very broad peak centred at 140 °C, which is obviously attributed to the PGOHMA homopolymer. In fact, PGOHMA is reported to have a T_g close to 105 °C as determined by DSC [47], which correlates with the obtained relaxation. In the case of PGOHMA-MBA/BC, the broad peak is centred at about 99 °C.

4. Conclusions

The simple and easy preparation of PGMA/BC nanocomposites *via* the *in-situ* free radical polymerization of GMA inside the BC network constitutes the first relevant contribution of this study. These nanocomposites present good thermal stability and viscoelastic properties, along with low water-uptake and crystallinity values due to the hydrophobic and amorphous PGMA matrix. The second novel feature of this work has to do with the post-polymerization treatment of the preformed PGMA/BC nanocomposites with hot hydrochloric acid to generate PGOHMA/BC nanocomposites by opening the epoxy ring to obtain materials with distinct properties, namely lower hydrophobicity and improved water-uptake capacity. Despite the lower crystallinity, the post-modified nanocomposites maintained their thermal stability, viscoelastic properties and porous structure. These results indicate that the PGMA/BC nanocomposites can be used as functional hydrophobic nanocomposites for post-modification reactions, whereas the PGOHMA/BC nanocomposites might have potentiality in biomedical applications requiring hydrophilic, swellable and possibly biocompatible materials such as hydrogels for drug delivery.

References

[1]   Z. Shi, Y. Zhang, G.O. Phillips, G. Yang, Utilization of bacterial cellulose in food, Food Hydrocoll. 35 (2014) 539–545. doi:10.1016/j.foodhyd.2013.07.012.

[2]   E. Pecoraro, D. Manzani, Y. Messaddeq, S.J.L. Ribeiro, Bacterial cellulose from Glucanacetobacter xylinus: Preparation, properties and applications, in: M.N. Belgacem, A. Gandini (Eds.), Monomers, Polym. Compos. from Renew. Resour., Elsevier, Amsterdam, 2008: pp. 369–383.

[3]   A.J.D. Silvestre, C.S.R. Freire, C.P. Neto, Do bacterial cellulose membranes have potential in drug-delivery systems?, Expert Opin. Drug Deliv. 11 (2014) 1113–1124. doi:10.1517/17425247.2014.920819.

[4]   H. Ullah, H.A. Santos, T. Khan, Applications of bacterial cellulose in food, cosmetics and drug delivery, Cellulose. 23 (2016) 2291–2314. doi:10.1007/s10570-016-0986-y.

[5]   H. Ullah, F. Wahid, H.A. Santos, T. Khan, Advances in biomedical and pharmaceutical applications of functional bacterial cellulose-based nanocomposites, Carbohydr. Polym. 150 (2016) 330–352. doi:http://dx.doi.org/10.1016/j.carbpol.2016.05.029.

[6]   H.G.O. Barud, R.R. Silva, H.S. Barud, A. Tercjak, J. Gutierrez, W.R. Lustri, O.B.O. Junior, S.J.L. Ribeiro, A multipurpose natural and renewable polymer in medical applications: Bacterial cellulose, Carbohydr. Polym. 153 (2016) 406–420. doi:10.1016/j.carbpol.2016.07.059.

[7]   M. Ul-Islam, S. Khan, M.W. Ullah, J.K. Park, Bacterial cellulose composites: Synthetic strategies and multiple applications in bio-medical and electro-conductive fields, Biotechnol. J. 10 (2015) 1847–1861. doi:10.1002/biot.201500106.

[8]   A.R.P. Figueiredo, C. Vilela, C.P. Neto, A.J.D. Silvestre, C.S.R. Freire, Bacterial

        cellulose-based nanocomposites: Roadmap for innovative materials, in: V.K.

        Thakur (Ed.), Nanocellulose Polym. Compos., Scrivener Publishing LLC, 2015:

        pp. 17–64.

[9]   M.L. Foresti, A. Vázquez, B. Boury, Applications of bacterial cellulose as

        precursor of carbon and composites with metal oxide, metal sulfide and metal

        nanoparticles: A review of recent advances, Carbohydr. Polym. 157 (2017) 447–

        467. doi:10.1016/j.carbpol.2016.09.008.

[10]   M. Faria, C. Vilela, A.J.D. Silvestre, B. Deepa, M. Resnik, C.S.R. Freire, N.

        Cordeiro, Physicochemical surface properties of bacterial

        cellulose/polymethacrylate nanocomposites: an approach by inverse gas

        chromatography, Carbohydr. Polym. 206 (2019) 86–93.

        doi:10.1016/j.carbpol.2018.10.110.

[11]   A.L. Buyanov, I. V Gofman, L.G. Revel'skaya, A.K. Khripunov, A.A.

        Tkachenko, Anisotropic swelling and mechanical behavior of composite bacterial

        cellulose-poly(acrylamide or acrylamide-sodium acrylate) hydrogels, J. Mech.

        Behav. Biomed. Mater. 3 (2010) 102–111. doi:10.1016/j.jmbbm.2009.06.001.

[12]   M.C.I.M. Amin, N. Ahmad, N. Halib, I. Ahmad, Synthesis and characterization

        of thermo- and pH-responsive bacterial cellulose/acrylic acid hydrogels for drug

        delivery, Carbohydr. Polym. 88 (2012) 465–473.

        doi:10.1016/j.carbpol.2011.12.022.

[13]   R. Hobzova, M. Duskova-Smrckova, J. Michalek, E. Karpushkin, P. Gatenholm,

        Methacrylate hydrogels reinforced with bacterial cellulose, Polym. Int. 61 (2012)

        1193–1201. doi:10.1002/pi.4199.

[14]   A.G.P.R. Figueiredo, A.R.P. Figueiredo, A. Alonso-Varona, S.C.M. Fernandes,

T. Palomares, E. Rubio-Azpeitia, A. Barros-Timmons, A.J.D. Silvestre, C.P. Neto, C.S.R. Freire, Biocompatible bacterial cellulose-poly(2-hydroxyethyl methacrylate) nanocomposite films, Biomed Res. Int. 698141 (2013) 1–14. doi:10.1155/2013/698141.

[15] T.D.O. Gadim, A.G.P.R. Figueiredo, N.C. Rosero-Navarro, C. Vilela, J.A.F. Gamelas, A. Barros-Timmons, C.P. Neto, A.J.D. Silvestre, C.S.R. Freire, F.M.L. Figueiredo, Nanostructured bacterial cellulose-poly(4-styrene sulfonic acid) composite membranes with high storage modulus and protonic conductivity, ACS Appl. Mater. Interfaces. 6 (2014) 7864–7875. doi:10.1021/am501191t.

[16] A.R.P. Figueiredo, A.G.P.R. Figueiredo, N.H.C.S. Silva, A. Barros-Timmons, A. Almeida, A.J.D. Silvestre, C.S.R. Freire, Antimicrobial bacterial cellulose nanocomposites prepared by in situ polymerization of 2-aminoethyl methacrylate, Carbohydr. Polym. 123 (2015) 443–453. doi:10.1016/j.carbpol.2015.01.063.

[17] C. Vilela, T.D.O. Gadim, A.J.D. Silvestre, C.S.R. Freire, F.M.L. Figueiredo, Nanocellulose/poly(methacryloyloxyethyl phosphate) composites as proton separator materials, Cellulose. 23 (2016) 3677–3689. doi:10.1007/s10570-016-1050-7.

[18] C. Vilela, N. Sousa, R.J.B. Pinto, A.J.D. Silvestre, F.M.L. Figueiredo, C.S.R. Freire, Exploiting poly(ionic liquids) and nanocellulose for the development of bio-based anion-exchange membranes, Biomass and Bioenergy. 100 (2017) 116–125. doi:10.1016/j.biombioe.2017.03.016.

[19] L. Saïdi, C. Vilela, H. Oliveira, A.J.D. Silvestre, C.S.R. Freire, Poly(N-methacryloyl glycine)/nanocellulose composites as pH-sensitive systems for controlled release of diclofenac, Carbohydr. Polym. 169 (2017) 357–365.

doi:10.1016/j.carbpol.2017.04.030.

[20]   C. Vilela, A.P.C. Martins, N. Sousa, A.J.D. Silvestre, F.M.L. Figueiredo, C.S.R.
        Freire, Poly(bis[2-(methacryloyloxy)ethyl] phosphate)/bacterial cellulose
        nanocomposites: Preparation, characterization and application as polymer
        electrolyte membranes, Appl. Sci. 8 (2018) 1145. doi:10.3390/app8071145.

[21]   H.Q. Pham, M.J. Marks, Epoxy Resins, in: Ullmann's Polym. Plast. Porducts
        Process., Wiley-VCH Verlag GmbH & Co. KGaA, 2016: p. 1669.

[22]   Q.-L. Li, W.-X. Gu, H. Gao, Y.-W. Yang, Self-assembly and applications of
        poly(glycidyl methacrylate)s and their derivatives, Chem. Commun. 50 (2014)
        13201−13215. doi:10.1039/C4CC03036B.

[23]   E.M. Muzammil, A. Khan, M.C. Stuparu, Post-polymerization modification
        reactions of poly(glycidyl methacrylate)s, RSC Adv. 7 (2017) 55874−55884.
        doi:10.1039/C7RA11093F.

[24]   M. Benaglia, A. Alberti, L. Giorgini, F. Magnoni, S. Tozzi, Poly(glycidyl
        methacrylate): a highly versatile polymeric building block for post-
        polymerization modifications, Polym. Chem. 4 (2013) 124−132.
        doi:10.1039/C2PY20646C.

[25]   M. Çelik, M. Önal, Synthesis and characterization of poly(glycidyl
        methacrylate)/Na-montmorillonite nanocomposites, J. Appl. Polym. Sci. 94
        (2004) 1532−1538. doi:10.1002/app.21075.

[26]   M. Žunić, A. Milutinović-Nikolić, A. Nastasović, Z. Vuković, D. Lončarević, I.
        Vuković, K. Loos, G. ten Brinke, D. Jovanović, Textural properties of
        poly(glycidyl methacrylate): Acid-modified bentonite nanocomposites, Polym.
        Bull. 70 (2013) 1805−1818. doi:10.1007/s00289-013-0924-1.

[27]   W. Wang, P. Julaiti, G. Ye, X. Huo, Y. Lu, J. Chen, Controlled architecture of

23

glass fiber/poly(glycidyl methacrylate) composites via surface-initiated ICAR ATRP mediated by mussel-inspired polydopamine chemistry, Ind. Eng. Chem. Res. 56 (2017) 11467–11476. doi:10.1021/acs.iecr.7b03065.

[28]   M. Martínez-Sanz, M.A. Abdelwahab, A. Lopez-Rubio, J.M. Lagaron, E. Chiellini, T.G. Williams, D.F. Wood, W.J. Orts, S.H. Imam, Incorporation of poly(glycidylmethacrylate) grafted bacterial cellulose nanowhiskers in poly(lactic acid) nanocomposites: Improved barrier and mechanical properties, Eur. Polym. J. 49 (2013) 2062–2072. doi:10.1016/j.eurpolymj.2013.04.035.

[29]   E. Trovatti, L.S. Serafim, C.S.R. Freire, A.J.D. Silvestre, C.P. Neto, Gluconacetobacter sacchari: An efficient bacterial cellulose cell-factory, Carbohydr. Polym. 86 (2011) 1417–1420. doi:10.1016/j.carbpol.2011.06.046.

[30]   S. Hestrin, M. Schramm, Synthesis of cellulose by Acetobacter xylinum - II. Preparation of freeze-dried cells capable of polymerizing glucose to cellulose, Biochem. J. 58 (1954) 345–352.

[31]   F. Jiang, Y.-L. Hsieh, Super water absorbing and shape memory nanocellulose aerogels from TEMPO-oxidized cellulose nanofibrils via cyclic freezing–thawing, J. Mater. Chem. A. 2 (2014) 350–359. doi:10.1039/C3TA13629A.

[32]   C. Tapeinos, E.K. Efthimiadou, N. Boukos, C.A. Charitidis, M. Koklioti, G. Kordas, Microspheres as therapeutic delivery agents: synthesis and biological evaluation of pH responsiveness, J. Mater. Chem. B. 1 (2013) 194–203. doi:10.1039/C2TB00013J.

[33]   H. Yang, J. Xu, S. Pispas, G. Zhang, One-step synthesis of hyperbranched biodegradable polymer, RSC Adv. 3 (2013) 6853–3858. doi:10.1039/c3ra23422c.

[34]   S. Yuan, J. Zhang, Z. Yang, S. Tang, B. Liang, S.O. Pehkonen, Click

functionalization of poly(glycidyl methacrylate) microspheres with triazole-4-carboxylic acid for the effective adsorption of Pb(II) ions, New J. Chem. 41 (2017) 6475–6488. doi:10.1039/C7NJ00797C.

[35]   L.J. Bellamy, The infrared spectra of complex molecules, 3rd ed., Chapman and Hall, Ltd., London, 1975.

[36]   P.S.S. Lacerda, A.M.M. V Barros-Timmons, C.S.R. Freire, A.J.D. Silvestre, C.P. Neto, Nanostructured composites obtained by ATRP sleeving of bacterial cellulose nanofibers with acrylate polymers, Biomacromolecules. 14 (2013) 2063–2073. doi:10.1021/bm400432b.

[37]   G.G. Godwin, C.S.J. Selvamalar, A. Penlidis, S. Nanjundan, Homopolymer of 4-propanoylphenyl methacrylate and its copolymers with glycidyl methacrylate: Synthesis, characterization, reactivity ratios and application as adhesives, React. Funct. Polym. 59 (2004) 197–209. doi:10.1016/j.reactfunctpolym.2004.01.010.

[38]   C. Lainé, V. Bounor-Legaré, C. Monnet, P. Cassagnau, Free radical polymerization of glycidyl methacrylate in plasticized Poly(vinyl chloride), Eur. Polym. J. 44 (2008) 3177–3190. doi:10.1016/j.eurpolymj.2008.07.004.

[39]   A.D. French, Idealized powder diffraction patterns for cellulose polymorphs, Cellulose. 21 (2014) 885–896. doi:10.1007/s10570-013-0030-4.

[40]   X. Yan, M. Li, J. Long, X. Zhang, H. Wei, Q. He, D. Rutman, D. Cao, S. Wei, G. Chen, Z. Guo, Highly monodisperse sub-microspherical poly(glycidyl methacrylate) nanocomposites with highly stabilized gold nanoparticles, Macromol. Chem. Phys. 215 (2014) 1098–1106. doi:10.1002/macp.201400097.

[41]   Y. Nishiyama, J. Sugiyama, H. Chanzy, P. Langan, Crystal structure and hydrogen bonding system in cellulose Iα from synchrotron X-ray and neutron fiber diffraction, J. Am. Chem. Soc. 125 (2003) 14300–14306.

doi:10.1021/ja037055w.

[42]   D.J. Haloi, P. Mandal, N.K. Singha, Atom transfer radical polymerization of glycidyl methacrylate (GMA) in emulsion, J. Macromol. Sci. Part A. 50 (2013) 121–127. doi:10.1080/10601325.2013.736270.

[43]   S. Zulfiqar, M. Zulfiqar, M. Nawaz, I.C. McNeill, J.G. Gorman, Thermal degradation of poly(glycidyl methacrylate), Polym. Degrad. Stab. 30 (1990) 195–203. doi:10.1016/0141-3910(90)90075-I.

[44]   T.D.O. Gadim, C. Vilela, F.J.A. Loureiro, A.J.D. Silvestre, C.S.R. Freire, F.M.L. Figueiredo, Nafion® and nanocellulose: a partnership for greener polymer electrolyte membranes, Ind. Crops Prod. 93 (2016) 212–218. doi:10.1016/j.indcrop.2016.01.028.

[45]   S.M. Safiullah, K.A. Wasi, K.A. Basha, Poly(glycidyl methacrylate) - A soft template for the facile preparation of poly(glycidyl methacrylate) core-copper nanoparticle shell nanocomposite, Appl. Surf. Sci. 357 (2015) 112–121. doi:10.1016/j.apsusc.2015.08.254.

[46]   H. Gao, M. Elsabahy, E. V. Giger, D. Li, R.E. Prud'Homme, J.C. Leroux, Aminated linear and star-shape poly(glycerol methacrylate)s: Synthesis and self-assembling properties, Biomacromolecules. 11 (2010) 889–895. doi:10.1021/bm901241k.

[47]   S.O. Kyeremateng, E. Amado, J. Kressler, Synthesis and characterization of random copolymers of (2,2-dimethyl-1,3-dioxolan-4-yl)methyl methacrylate and 2,3-dihydroxypropyl methacrylate, Eur. Polym. J. 43 (2007) 3380–3391. doi:10.1016/j.eurpolymj.2007.04.048.

[48]   D.M. Yu, J.K.D. Mapas, H. Kim, J. Choi, A.E. Ribbe, J. Rzayev, T.P. Russell, Evaluation of the interaction parameter for poly(solketal methacrylate)-block -

polystyrene copolymers, Macromolecules. 51 (2018) 1031–1040.

doi:10.1021/acs.macromol.7b02221.

[49]   S.E. Shaw, T. Russo, D.H. Solomon, G.G. Qiao, An alternative pathway for the

hydrolysis of epoxy ester compounds, Polymer. 47 (2006) 8247–8252.

doi:10.1016/j.polymer.2006.10.004.

[50]   P. Soulounganga, C. Marion, F. Huber, P. Gerardin, Synthesis of poly(glycerol

methacrylate) and its application to dimensional stabilization of wood, J. Appl.

Polym. Sci. 88 (2003) 743–749. doi:10.1002/app.11510.

Tables

Table 1. Composition in weight fraction of the prepared nanocomposites in the dry
state.

Nanocomposites	Nominal composition		Measured composition		
	W_{GMA}/W_{BC}	W_{MBA}/W_{GMA}	W_{PGMA}/W_{BC}	W_{BC}/W_{total}	W_{PGMA}/W_{total}
PGMA/BC	2.0	0.0	1.56	0.39	0.61
PGMA-MBA/BC	2.0	0.2	2.03	0.33	0.67

Figure captions

Figures

Fig. 1. Radical polymerization of GMA in the a) absence and b) presence of cross-linker (MBA), and c) post-polymerization treatment: acid catalysed diol formation from the epoxy groups of PGMA.
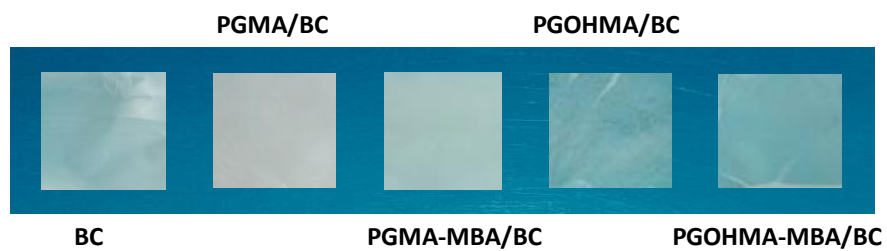
Fig. 2. Photographs of pure BC, PGMA- and PGOHMA-based nanocomposites.
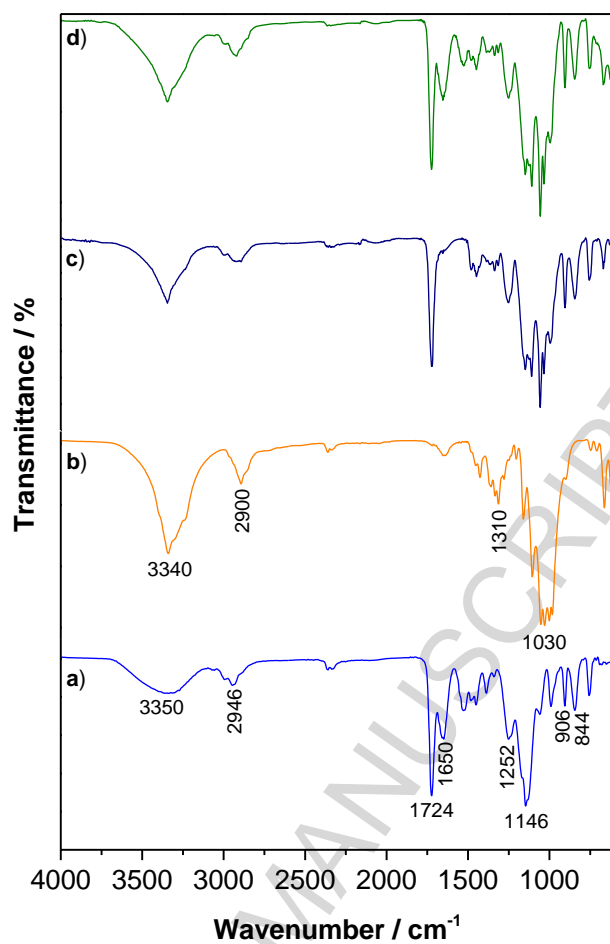
Fig. 3. FTIR-ATR spectra of a) cross-linked PGMA, b) BC, and nanocomposites c) PGMA/BC and d) PGMA-MBA/BC.
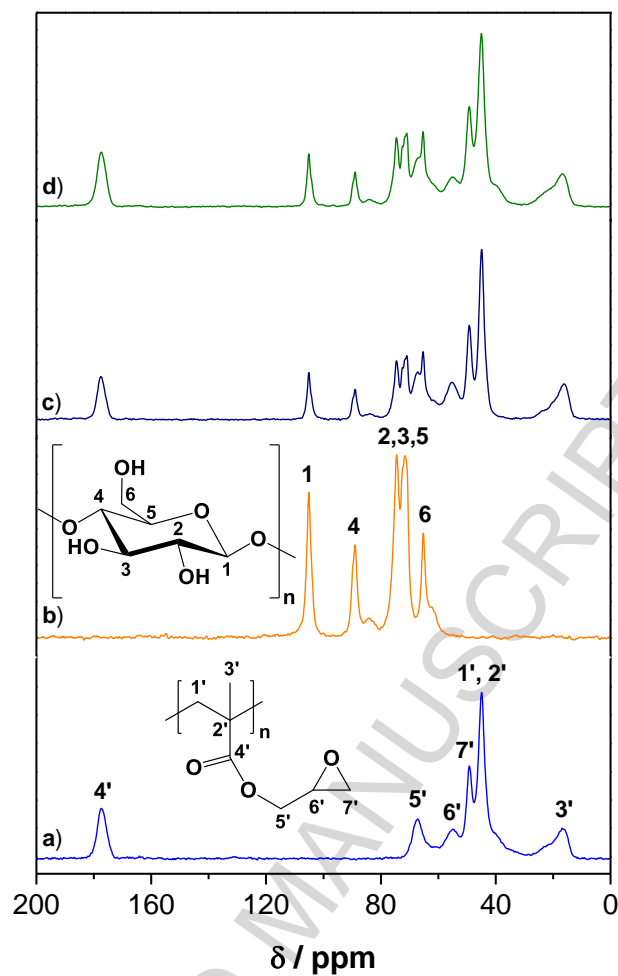
Fig. 4. ^{13}C CP/MAS NMR spectra of a) cross-linked PGMA, b) BC and nanocomposites c) PGMA/BC and d) PGMA-MBA/BC.
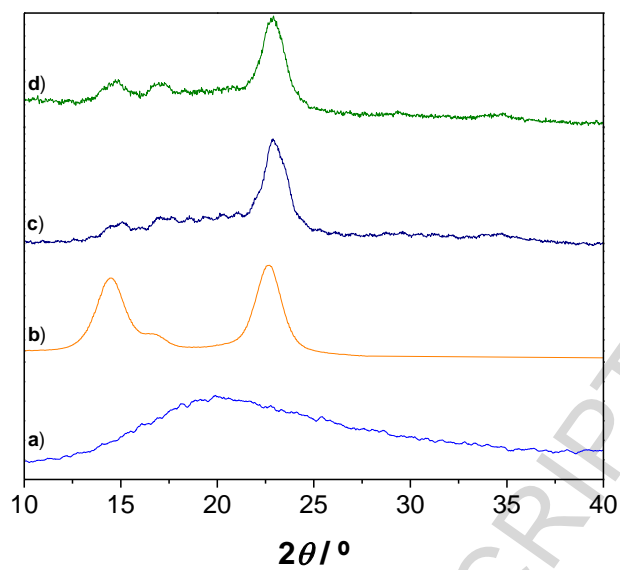
Fig. 5. X-ray diffractograms of a) cross-linked PGMA, b) BC and nanocomposites c) PGMA/BC and d) PGMA-MBA/BC.
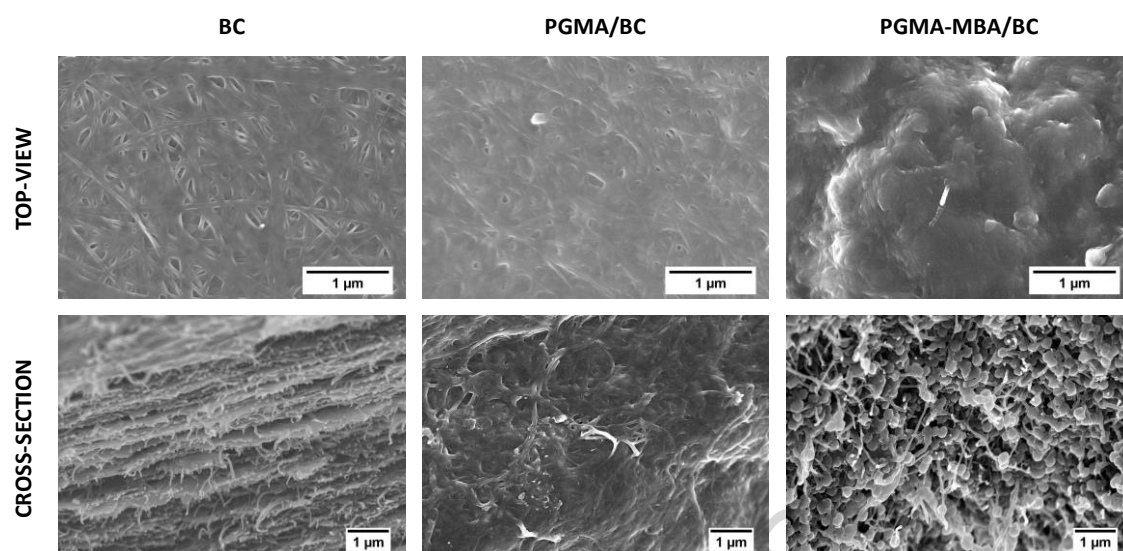
Fig. 6. Top-view (top) and cross-section (bottom) micrographs of BC and nanocomposites PGMA/BC and PGMA-MBA/BC.
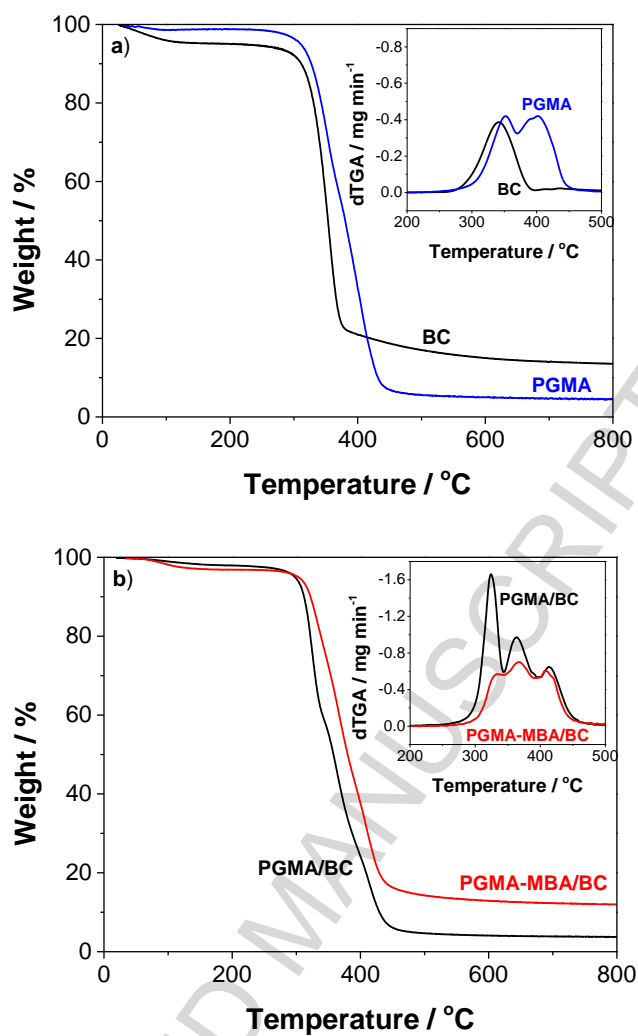
Fig. 7. Thermograms of a) cross-linked PGMA and neat BC, and b) nanocomposites PGMA/BC and PGMA-MBA/BC. The inset curves correspond to the derivative.
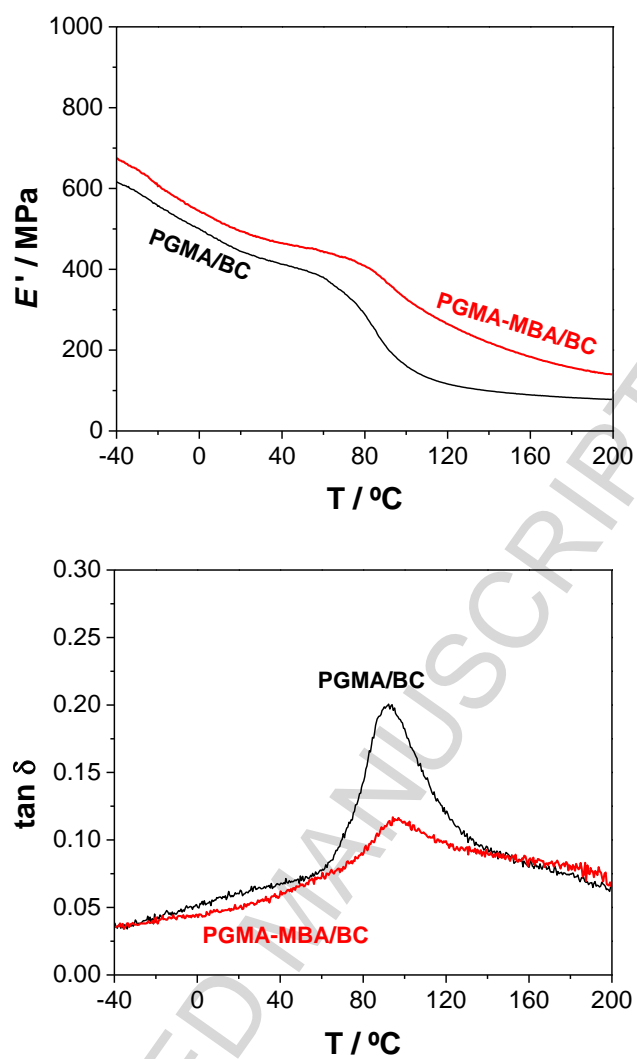
Fig. 8. Storage modulus (*E'*, top) and loss factor (tan *δ*, bottom) curves of nanocomposites PGMA/BC and PGMA-MBA/BC.
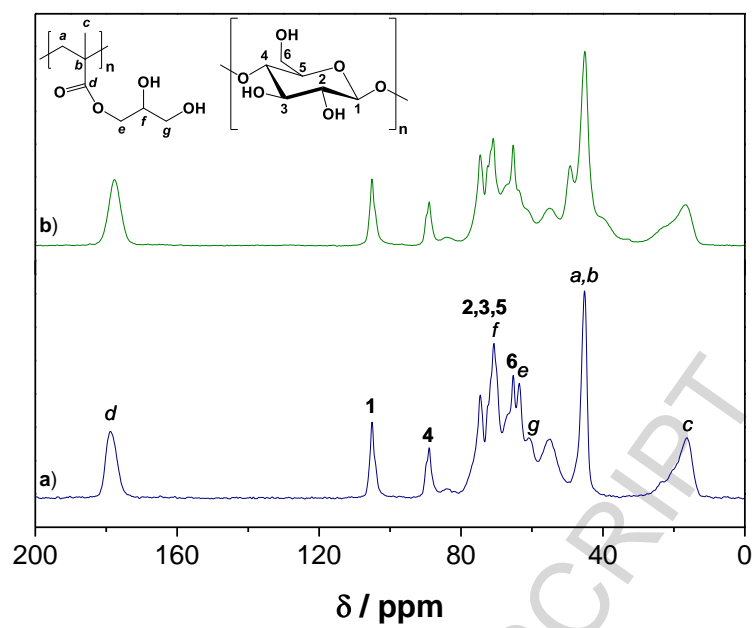
Fig. 9. ^{13}C CP/MAS NMR spectra of nanocomposites a) PGOHMA/BC and b) PGOHMA-MBA/BC.

38

PGOHMA/BC   **PGOHMA-MBA/BC**
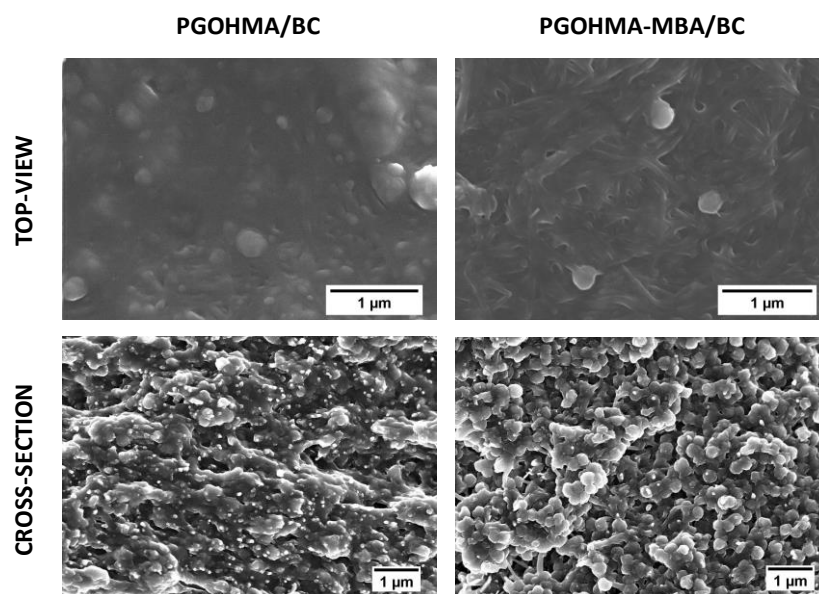
Fig. 10. Top-view (top) and cross-section (bottom) micrographs of the preformed nanocomposites after the acidic heat treatment: PGOHMA/BC and PGOHMA-MBA/BC.
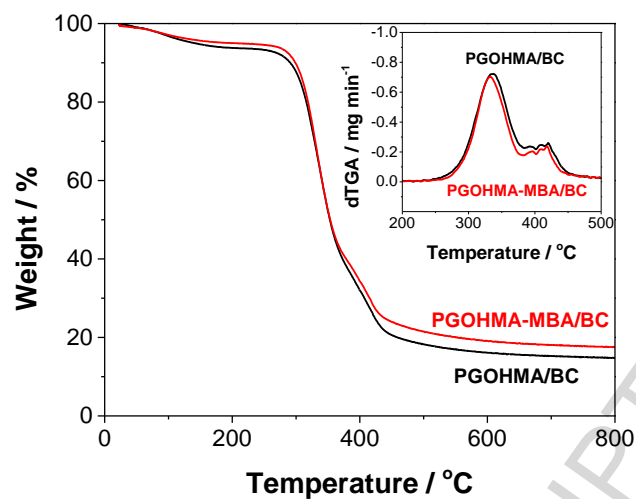
Fig. 11. Thermograms of nanocomposites PGOHMA/BC and PGOHMA-MBA/BC. The inset curves correspond to the derivative.
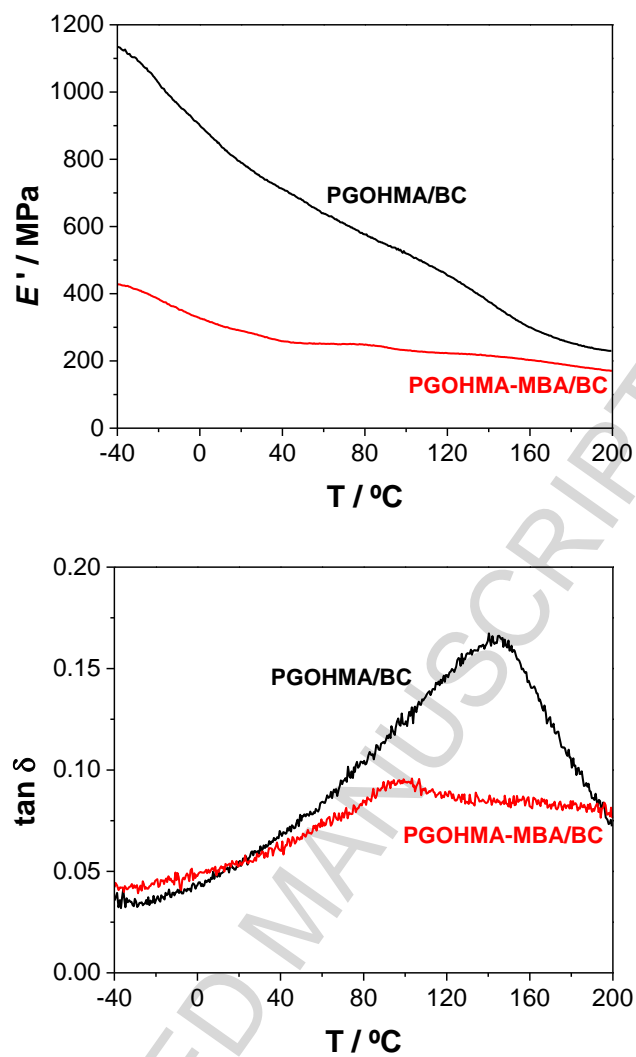
Fig. 12. Storage modulus (*E'*, top) and loss factor (tan *δ*, bottom) curves for nanocomposites PGOHMA/BC and PGOHMA-MBA/BC.

Highlights

- Poly(glycidyl methacrylate) (PGMA)/bacterial cellulose (BC) nanocomposites were prepared.

- Unique features of BC improved the properties of the functional PGMA/BC nanocomposites.

- Hydrophobic PGMA/BC nanocomposites have potential for post-modification reactions.

- Post-modification originated poly(glyceryl methacrylate) (PGOHMA)/BC nanocomposites.

- Hydrophilic PGOHMA/BC nanocomposites with potential for biomedical applications.
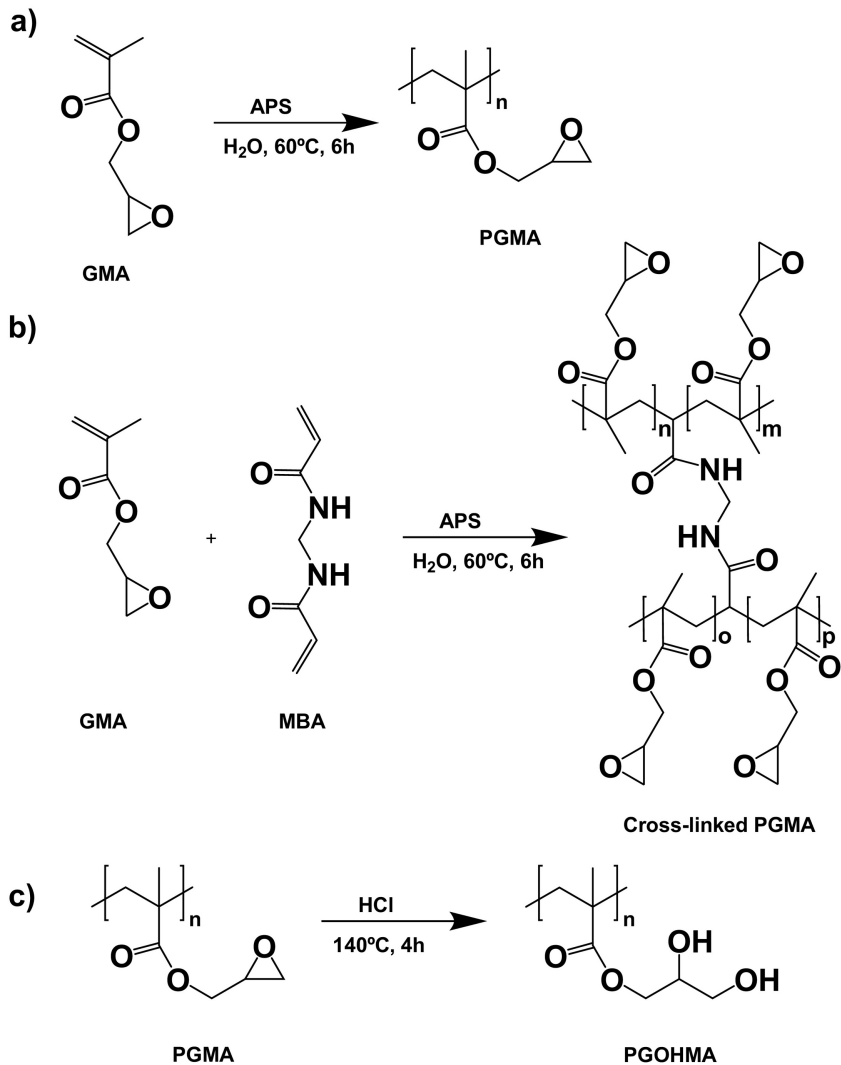
Figure 1
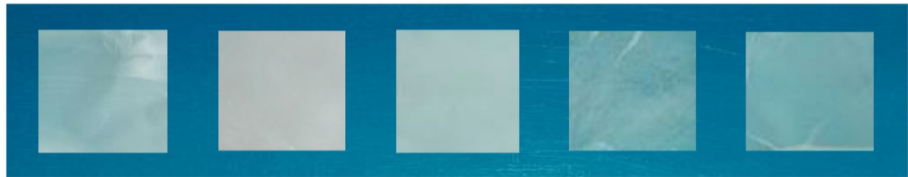
Figure 2

Figure 3

Figure 4

d)

c)

b)

a)

2θ / °
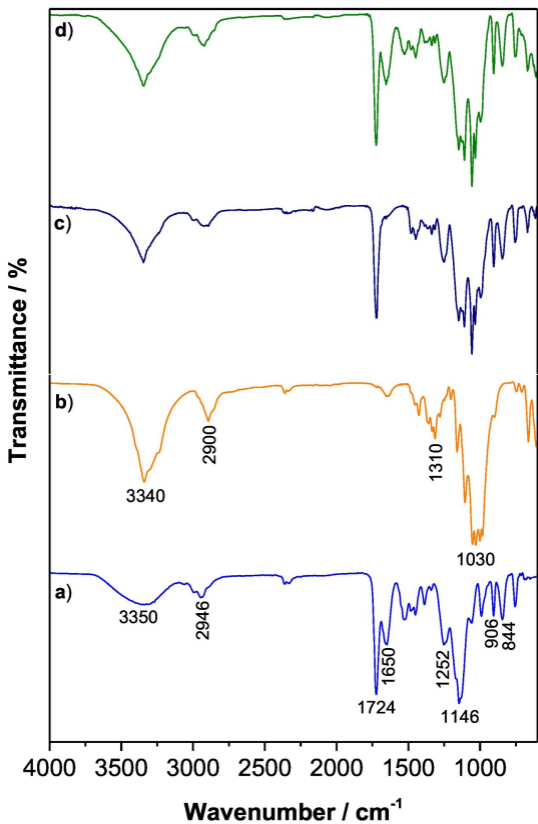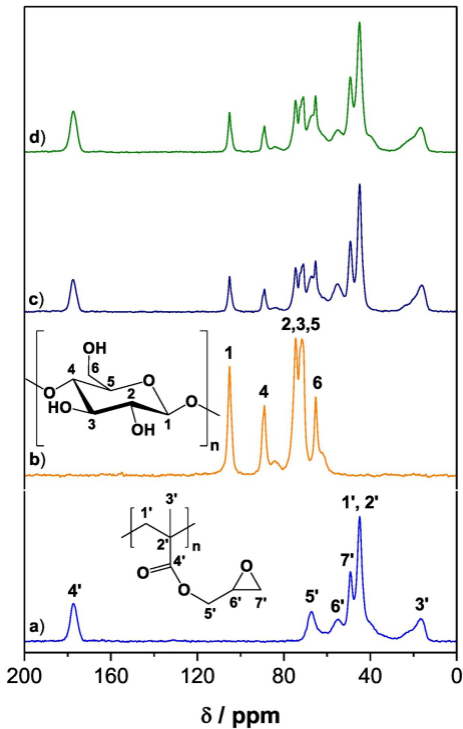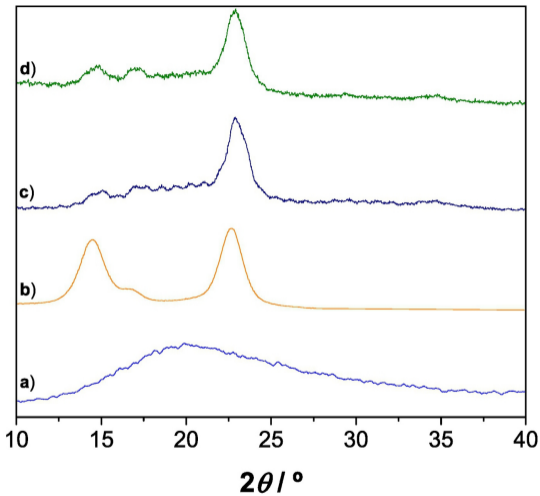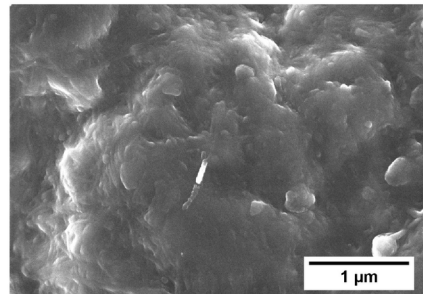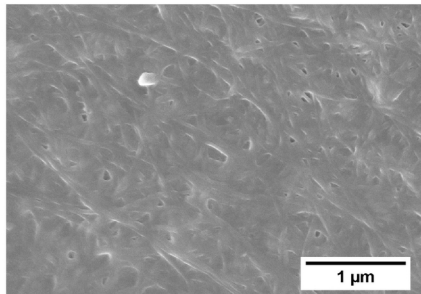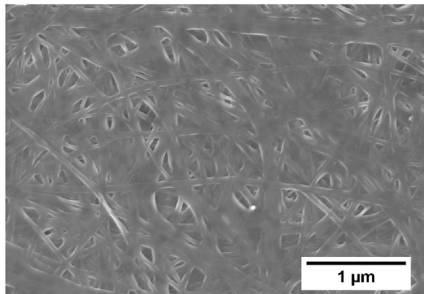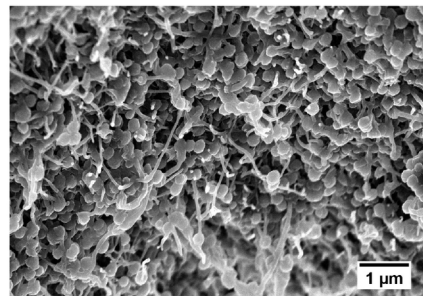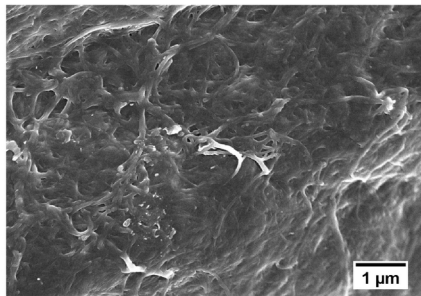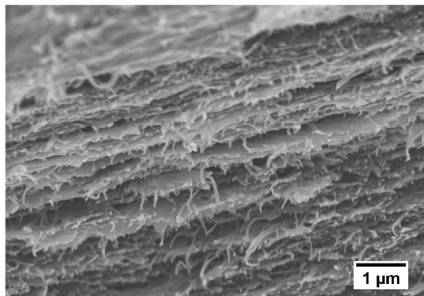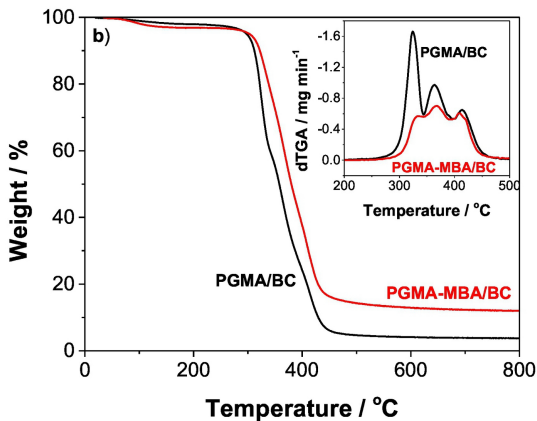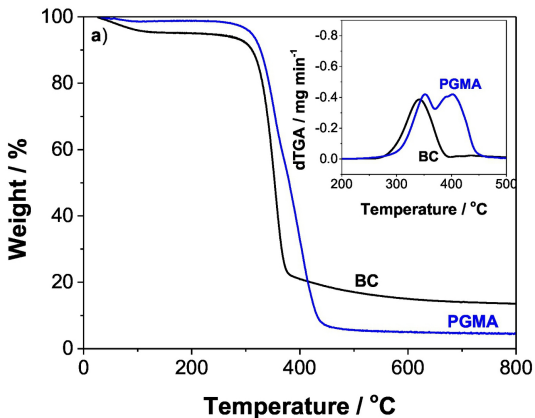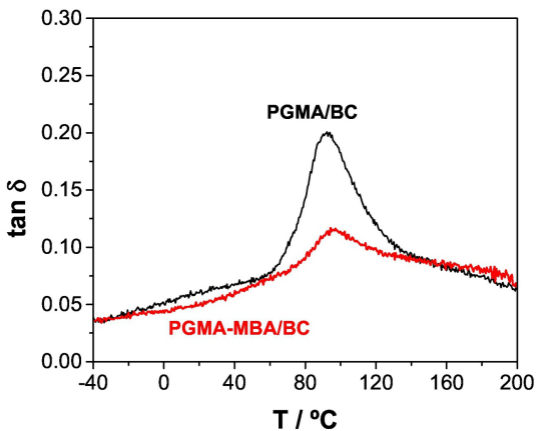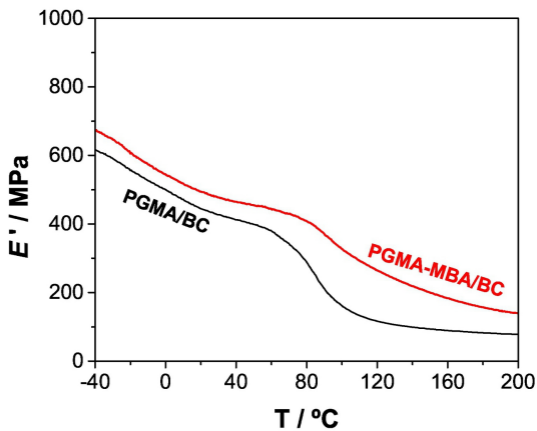
Figure 5

Figure 6

Figure 7

Figure 8
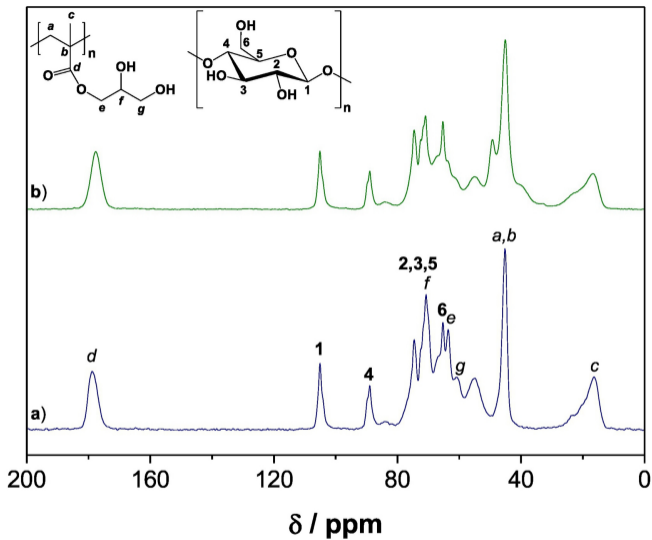
Figure 9
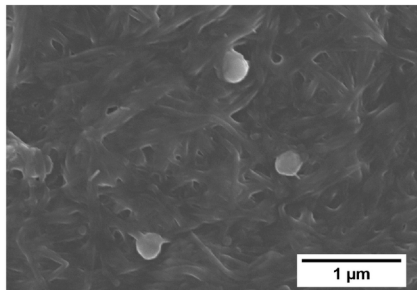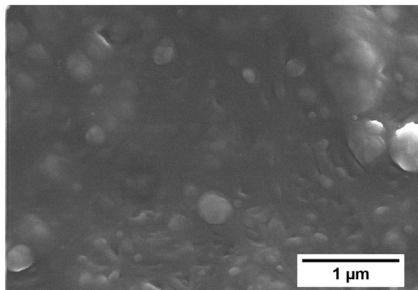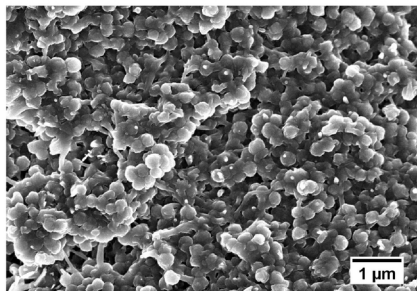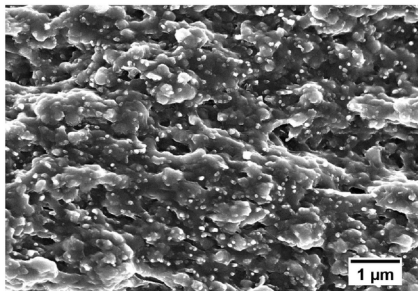
Figure 10

Figure 11

Figure 12